Cerium oxide nanoparticles inside carbon nanoreactors for selective allylic oxidation of cyclohexene

Nityananda Agasti [a†], *Maxwell A. Astle* [a]*, *Graham A. Rance* [a,b], *Jesum Alves Fernandes* [a], *Jairton Dupont* [a,c] *Andrei N. Khlobystov* [a,b]*

[a] School of Chemistry, University of Nottingham, University Park, Nottingham, NG7 2RD, United Kingdom.

[b] Nanoscale and Microscale Research Centre (nmRC), University of Nottingham, University Park, Nottingham, NG7 2RD, United Kingdom.

[c] Univ Fed Rio Grande do Sul, Inst Chem, Ave Bento Goncalves 9500, BR-91501970 Porto Alegre, RS, Brazil.

KEYWORDS

CeO_2 nanoparticles, carbon nanotubes, nanoreactors, alkene oxidation, nanocatalysis

ABSTRACT

The confinement of cerium oxide nanoparticles within hollow carbon nanostructures has been achieved and harnessed to control the oxidation of cyclohexene. Graphitised carbon nanofibres (GNF) have been used as the nanoscale tubular host and filled by sublimation of the $Ce(tmhd)_4$ complex (where tmhd = tetrakis(2,2,6,6-tetramethyl-3,5-heptanedionato)) into the internal cavity, followed by a subsequent thermal decomposition to yield the hybrid nanostructure CeO_2@GNF, where nanoparticles are preferentially immobilised at the internal graphitic step-edges of the GNF. Control over the size of the CeO_2 nanoparticles has been demonstrated within the range c.a. 4 to 9 nm by varying the mass ratio of the $Ce(tmhd)_4$ precursor to GNF during the synthesis. CeO_2@GNF were effective in promoting the allylic oxidation of cyclohexene, in high yield, with time-dependent control of product selectivity, at a comparatively low loading of CeO_2 of 0.13 mol%. Unlike many of the reports to date where ceria catalyses such organic transformations, we found the encapsulated CeO_2 to play the key role of radical initiator due to the presence of Ce^{3+} included in the structure, with the nanotube acting as both a host, preserving the high performance of the CeO_2 nanoparticles, anchored at the GNF step-edges, over multiple uses, and an electron reservoir, maintaining the balance of Ce^{3+} and Ce^{4+} centers. Spatial confinement effects ensure excellent stability and recyclability of CeO_2@GNF nanoreactors.

INTRODUCTION

Lanthanide compounds continue to attract significant attention owing to their unusual magnetic, redox and optical properties, different to d-block elements, which is attributed to the nature of the 4f orbitals, buried deep inside the atom and thus shielded from the external environment by the overlying 5s and 5p orbitals. This contracted nature of the 4f orbitals gives lanthanides their unique physicochemical properties and underpins a wide range of applications in catalysis,[1] magnetism[2] and pharmacology.[3] Among these, catalysis alone represents nearly 75% of the total applications of the lanthanides. As a catalyst, cerium (Ce), unlike most of the other lanthanides,[4] is utilised in the form of its oxide (CeO_2), also known as ceria, with a wide range of ceria-based nanocatalysts, including spheres,[5] rods,[6] tubes,[7] wires,[8] shuttle-shaped[9] and flower-like nanoparticles,[8] reported over the last decade. The remarkable catalytic behaviour of ceria observed ubiquitously throughout these nanostructures is due to the interconversion between Ce^{4+} and Ce^{3+}, controllable by the reaction conditions, with CeO_2 and Ce_2O_3 observed under oxidising and reducing conditions, respectively. As a consequence of this interconversion, CeO_2 can reversibly release oxygen from its structure at moderate temperatures (<600ºC)[10] leading to the formation of oxygen vacancies in the crystal lattice and simultaneous reduction of Ce^{4+} to Ce^{3+}. This behaviour makes ceria extremely useful for oxygen storage and release applications,[11] as well as in other important chemical reactions, such as the preparation of imines,[12] the oxidation of CO to CO_2[13] and the hydrogenation of CO_2 to methanol.[14] However, a less explored and often disregarded application of ceria is its ability to initiate radical-mediated organic transformations, which often commence in the homolytic cleavage of organic peroxides by Ce^{3+}, as demonstrated in the oxidation of cyclohexene, [15] the products of which represent important intermediates in the chemical industry.[16] Akin to the structure-function relationships observed in ceria nanocatalysis, the shape and size of

ceria nanoparticles are expected to modulate its efficiency as an initiator; [17, 18] yet, further research is critically required to probe how the physical and chemical properties of CeO_2 influence the yields and distribution of products of radical-based chemical reactions.

Despite the breadth of ceria-based nanostructures synthesised to date, the controllable preparation of monodisperse ultra-small CeO_2 nanoparticles remains a significant challenge. Moreover, preservation of their functional properties by preventing deactivation under harsh reaction conditions is essential for their further development. One recent approach to address the latter concerns the encapsulation of CeO_2 nanoparticles in core-shell and yolk-shell structures, where CeO_2 is protected by an outer shell, which was shown as an efficient way to stabilise CeO_2 nanoparticles and explore the effect of spatial confinement at the nanoscale.[19,20] However, carbon nanotubes (CNTs) as a host matrix for the confinement of CeO_2 nanoparticles have the potential to solve both of these challenges. Besides being a container with two dimensions on the nanoscale and thus the capacity to template the formation of particles with nanoscopic sizes, the remarkable mechanical (tensile strength much higher than that of steel), thermal (stable up to ca. 600ºC in air and up to 2800ºC in vacuum or inert atmosphere) and chemical stability of CNTs makes them an excellent candidate support material for nanoparticles under a wide variety of reaction conditions.[21] In addition, the curvature of the CNT walls causes re-distribution of the π electron density of graphene layers from the concave inner to the convex outer surface resulting in an electron density gradient. As a consequence, encapsulated metal nanoparticles inside carbon nanotubes often exhibit properties distinct from those adsorbed on the CNT outside surface.[22] Therefore, the encapsulation of metal or metal oxide nanoparticles inside CNTs opens a pathway towards active nanoreactors with tuneable properties, such as those reported by our group[23,24] and others previously.[25,26]

While several examples of the successful deposition of CeO_2 nanoparticles onto the outer surface of carbon nanotubes (CeO_2-CNT) have been reported and applied in catalysis,[27,28] biosensing[29,30] and as a fuel additive,[31] the preparation of ceria nanoparticles inside carbon nanotubes remains largely unexplored, with only one example to date reported for CeO_2 nanoparticles inside carbon nanotubes of inner diameter 4-8 nm.[32] Such narrow nanotubes serve as excellent model systems for catalyst supports, but their applications for preparative scale reactions are limited. In this study, we utilised graphitised carbon nanofibres (GNF) that have many of the attractive properties of carbon nanotubes, but with the added benefits of (i) large internal diameters (typically larger than 60 nm) enabling the efficient mass transport of reactants and products to and from the internal cavity and (ii) corrugated internal surfaces resulting in the effective stabilisation of nanoparticles, as demonstrated in our previous studies (Figure 1).[33-36] Herein, successfully prepared ceria nanoparticles within GNF (CeO_2@GNF) were analysed by a variety of structural and chemical characterisation techniques, and applied in the preparative-scale reaction of cyclohexene oxidation, revealing key features of nanoscale confinement in carbon nanoreactors important for sustainable organic synthesis.

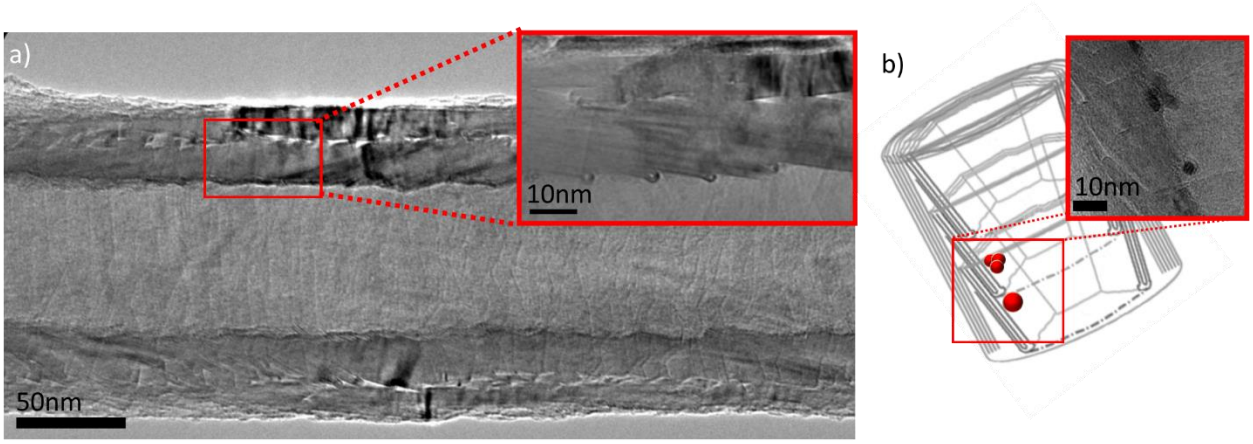

Figure 1. (a) Low and high magnification (inset) high resolution transmission electron microscopy (HRTEM) images of empty hollow graphitised carbon nanofibres (GNF). As shown in both the electron micrographs in (a) and the schematic representation

in (b), GNF are topologically complex nanoscale structures comprising a series of stacked cups encased within concentric tubes. The internal diameters are much larger than the dimensions of simple molecular species (typically by more than an order of magnitude) and the termini are always open, thus facilitating highly efficient transport of molecules through the internal volume. Furthermore, the 3-4 nm high folds on the interior surfaces of GNF formed by rolled-up sheets of graphene provide exemplary anchoring points for guests, such as molecules and nanoparticles, as shown in (b), due to maximised van der Waals interactions. This creates localised nanoscale reaction environments, different to the bulk phase, which impart spatial restrictions and thus can significantly impact the yields and distributions of products afforded across a range of preparative chemical transformations, as demonstrated by us and others.[37-48]

EXPERIMENTAL SECTION

General

All reagents and solvents were purchased from Sigma-Aldrich, including cyclohexene (>99%) and were used as received. Graphitised carbon nanofibres (GNF) and tetrakis(2,2,6,6-tetramethyl-3,5-heptanedionato) cerium (IV) (99.9% Ce) were purchased from Pyrograf Products, USA and Strem Chemicals, USA, respectively. Graphite flakes (Code G/0900/60, Batch 043775) and activated carbon (Activated Charcoal, DARCO) were purchased from Fisher Scientific. All glassware was cleaned with a mixture of hydrochloric and nitric acid (3:1 v/v, "aqua regia") and rinsed thoroughly with deionised water, cleaned with potassium hydroxide in isopropyl alcohol and finally rinsed thoroughly with deionised water before use. Prior to use, GNF was ball milled using a Retsch MM40 Ball Miller with 5 mL jars and 12 mm stainless steel balls at a frequency of 10 per second for 90 minutes.

Preparation of CeO_2 nanoparticles encapsulated within graphitised carbon nanofibres (CeO_2@GNF) and deposited on graphite (CeO_2@graphite) and activated carbon (CeO_2@AC)

Graphitised carbon nanofibres (10 mg, PR19-XT-HHT, ball-milled) and $Ce(tmhd)_4$ (1, 2 or 3 mg) were sealed in a Pyrex glass ampoule under vacuum (2.9×10^{-5} mbar) and heated at 150 ºC in an oil bath for 72 hours to allow for sublimation of the cerium complex and diffusion inside the channels of GNF. After 72 hours, the ampoule was quickly cooled by placing into ice cold water for 10 minutes before opening. The obtained bulk solid was then placed in another Pyrex glass ampoule, evacuated at 1.6×10^{-2} mbar and backfilled with argon (this procedure was repeated three times to ensure removal of molecular oxygen and atmospheric moisture), and the ampoule was then sealed and heated at 600 ºC for 2 hours to decompose the cerium complex to CeO_2, followed by slow cooling for 8 hours to a final temperature of 20 ºC to yield the resultant CeO_2@GNF-X material (where X = 1, 2 or 3 corresponding to the mass of cerium complex used in the initial step). The CeO_2@graphite and CeO_2@AC nanocomposite was prepared using an analogous method with graphite powder or activated carbon (AC) and $Ce(tmhd)_4$ in a mass ratio of 10:2 (mg), to serve as a reference for CeO_2@GNF-2.

Characterisation of CeO_2@GNF, CeO_2@graphite and CeO_2@AC

High resolution transmission electron microscopy (HRTEM) was performed using a JEOL 2100F transmission electron microscope (field emission electron gun source, information limit 0.19 nm). Energy dispersive X-ray (EDX) analysis was performed using an Oxford Instruments INCA 560 X-ray microanalysis system. TEM samples were prepared by dispersing small quantities in methanol with bath sonication for 30 seconds to 1 minute, before drop-casting onto a copper TEM grid coated with a lacey carbon film (Agar Scientific UK) and drying in air. Particle size and *d*-spacing were determined using Gatan Digital Micrograph software. Thermogravimetric analysis (TGA) of samples was carried out using a TA Q500 Thermogravimetric Analyser. All samples were deposited onto platinum pans and analysed in air at a heating rate of 10ºC/min from 20 to

1000ºC with an isotherm for 10 min at 1000ºC, and airflow of 60mL/min. Raman spectroscopy was performed using a Horiba-Jobin-Yvon LabRAM HR spectrometer. Spectra were acquired using a 532 nm laser (at 0.3 mW power) and a 600 lines mm^{-1} rotatable diffraction grating, conferring a spectral resolution of better than 1.8 cm^{-1}. Spectra were baseline corrected using a linear fitting model. The powder X-ray diffraction (PXRD) patterns were recorded using a PANalytical X'Pert Pro diffractometer equipped with a Cu K(α) radiation source (λ = 1.5432 Å, at 40kV and 40mA) in Bragg-Brentano geometry using a Si zero background holder. A few drops of isopropyl alcohol were added to all samples for good adhesion to the sample holder. The parameters for a typical measurement were as follows: start angle 5º, stop angle 120º, step size 0.0525º, time/step 6080s, scan speed 0.002200/s. X-ray photoelectron spectroscopy (XPS) measurements were performed using a Kratos AXIS Ultra DLD instrument. The chamber pressure during the measurements was 5×10^{-9} Torr. Wide energy range survey scans were collected at a pass energy of 80 eV in hybrid slot lens mode and a step size of 0.5 eV over 20 min. The charge neutraliser filament was used to prevent the sample from charging over the irradiated area. The X-ray source was a monochromated Al *Kα* emission, run at 10 mA and 12 kV (120 W). The energy range for each 'pass energy' (resolution) was calibrated using the Kratos Cu $2p_{3/2}$, Ag $3d_{5/2}$ and Au $4f_{7/2}$ three-point calibration method. The transmission function was calibrated using a clean gold sample method for all lens modes and the Kratos transmission generator software within Vision II. The data were processed with CASAXPS (Version 2.3.17). The high resolution data was charge corrected to the reference C 1s signal at 284.5 eV.

Oxidation of cyclohexene

The oxidation of cyclohexene with *tert*-butylhydroperoxide (TBHP, 70 wt% in H_2O) was carried using either CeO_2@GNF, CeO_2@graphite or CeO_2@AC in a two-necked glass round-bottom flask

equipped with a magnetic stirrer and a reflux condenser open to air. In a typical reaction, a mixture of cyclohexene (2.9 mmol), TBHP (5.8 mmol), CeO_2@Y (10 mg, where Y = GNF, graphite or AC, containing 0.09-0.18 mol % CeO_2) and 1,4-dichlorobenzene (1.4 mmol) as an internal standard were dispersed in acetonitrile (2.5 mL) and stirred at 80 °C. The progress of the reaction was followed using ^{1}H NMR spectroscopy. To study the reaction kinetics, aliquots (0.01 mL) were taken from the reaction mixture at one hour intervals. Confirmation of the final products was determined using ^{1}H NMR spectroscopy. For recycling studies, the catalyst was recovered by filtration, washed with methanol and dried overnight before repeating the procedure for oxidation of cyclohexene. The same reaction conditions mentioned above with freshly loaded reactants. The recycling reaction was conducted five times for CeO_2@GNF.

RESULTS AND DISCUSSION

Growth of CeO_2 nanoparticles inside GNF (CeO_2@GNF)

CeO_2 nanoparticles encapsulated inside graphitised carbon nanofibres (CeO_2@GNF) have been prepared by heating a volatile precursor deposited within GNF (**Scheme 1**).

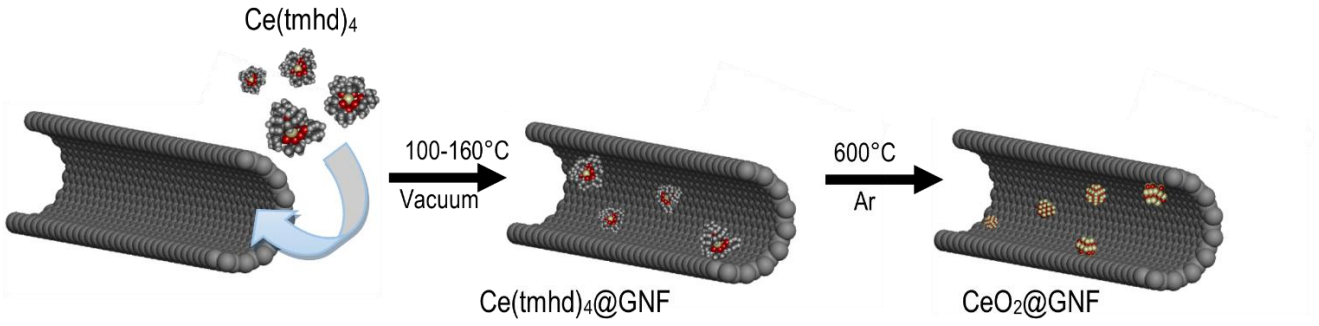

Scheme 1. Schematic illustration depicting the preparation of CeO_2 nanoparticles inside graphitised carbon nanofibres by initial sublimation under vacuum and subsequent thermal decomposition of the cerium complex, tetrakis(2,2,6,6-tetramethyl-3,5-heptanedionato)cerium(IV) [$Ce(tmhd)_4$] into cerium oxide, CO and CO_2 in an inert atmosphere.

Prior to filling, graphitised carbon nanofibres were ball milled to reduce their length from more than 10 µm to around 1.2 µm to reduce the possible impact of length-dependent transport resistance of reactant molecules from the bulk liquid-phase when later applied as a nanoreactor. The precursor $Ce(tmhd)_4$ was mixed with milled GNF, sealed under vacuum in a glass ampoule and heated above its sublimation temperature to ensure the diffusion of $Ce(tmhd)_4$ vapour into the channel of GNF, forming the [$Ce(tmhd)_4$@GNF] composite. The ampoule was then rapidly cooled in a cold water reservoir to facilitate the condensation of the precursor molecules inside GNF.[48] The [$Ce(tmhd)_4$@GNF] composite was subsequently heated under an argon atmosphere at a temperature above the decomposition point of the $Ce(tmhd)_4$, in this case 600 ºC, (Figure S1, SI) yielding CeO_2 nanoparticles inside GNF. In order to study the effect of precursor concentration on the formation of CeO_2 nanoparticles, three different amounts of the cerium complex (1, 2 and 3 mg) have been used with a fixed mass of GNF (10 mg) under the same reaction conditions.

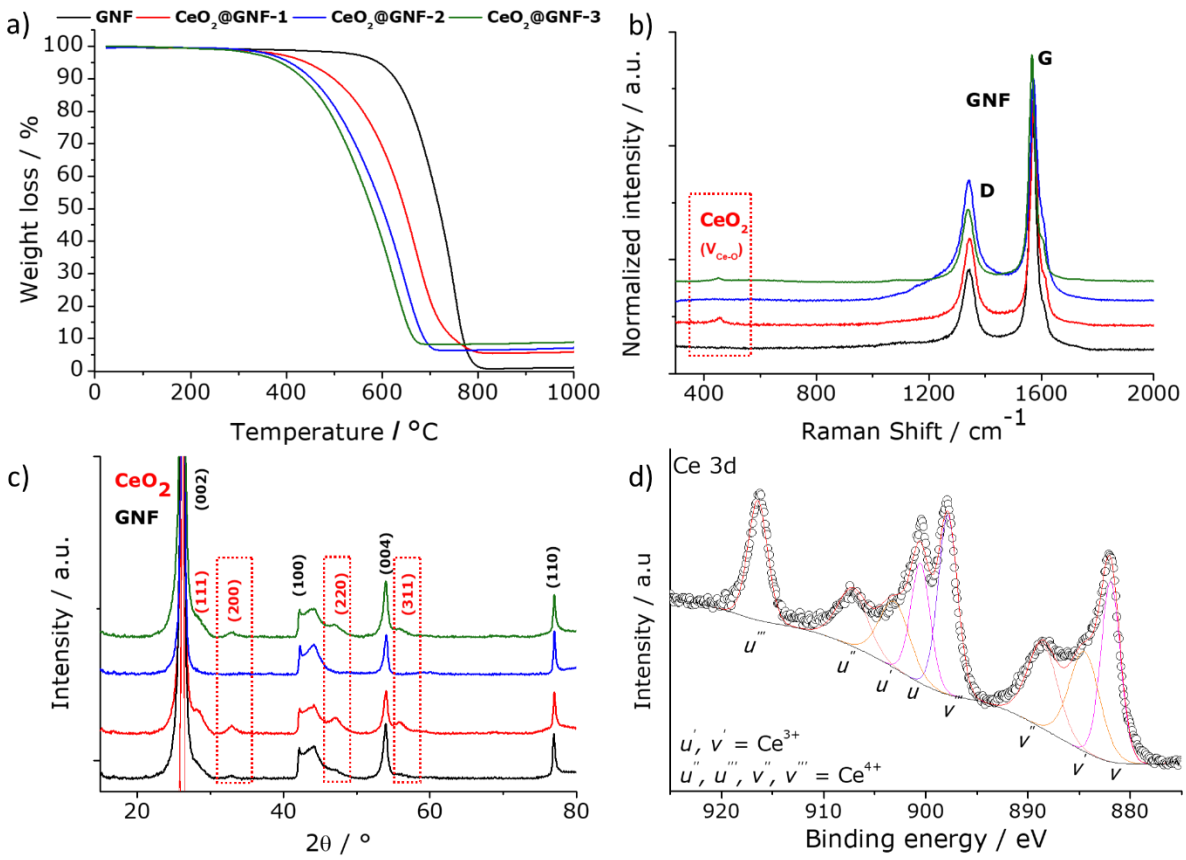

Figure 2. (a) TGA, (b) Raman spectroscopy, (c) PXRD and d) XPS analysis of the CeO_2@GNF nanocomposites. A decrease in the GNF combustion temperature and increase in the residual mass of CeO_2 obtained after GNF combustion observed in the thermograms (a) both correlate with the increasing amount of cerium complex used in the initial step. The Raman spectra (b) and PXRD patterns (c) of the CeO_2@GNF nanocomposites both confirm the presence of both GNF and CeO_2. Traces in (b) and (c) have been offset on the y-axis for visual clarity. The Raman spectra in (b) have been normalised to the intensity of the G-band. Annotated labels in (b) and (c) indicate Raman bands and diffraction planes corresponding to CeO_2 (red) and GNF (black). The fitted peak envelope for Ce 3d (d) in the XP spectrum confirms the presence of Ce^{3+} which can act as an initiator in the reaction of cyclohexene and TBHP.

To ascertain the loading of ceria in the CeO_2@GNF nanocomposites and to study the resultant GNF thermal stability, thermogravimetric analysis was conducted (**Figure 2a**). For all three CeO_2@GNF samples, a single weight loss, representing ~92-95% of the total weight and

corresponding to the combustion of GNF, was observed. The residual weight subsequent to GNF combustion (4.7, 5.9 and 7.7 %) is associated with CeO_2 loading and correlates well with the initial amount of cerium precursor added to GNF (1, 2 and 3 mg, respectively). It is interesting to note that the GNF combustion temperature for CeO_2@GNF is much lower (~625-675 ^oC) than that of empty GNF (~750 ^oC). This decreases with increasing CeO_2 loading and indicates a catalytic effect of CeO_2 on the oxidation of graphitic carbon in air.[49,50] This observation supports the notion that CeO_2 is an effective catalyst of oxidation due to the reversible loss of oxygen and interconversion of Ce^{4+} and Ce^{3+}, thus facilitating the combustion of GNF at a lower temperature.[31] TGA profiles also indicate a uniform one-step oxidation process, which is consistent with a homogeneous composition of the total CeO_2@GNF sample, i.e. negating the independent formation of CeO_2 and GNF in isolation.

The Raman spectra of CeO_2@GNF (**Figure 2b**) are dominated by two characteristic GNF bands: the G (graphitic) band – a carbon-carbon stretching vibration of E_{2g} symmetry, typically observed in graphitic nanocarbons – at ~1580 cm^{-1} and the D (disorder) band – a ring-breathing mode of A_{1g} symmetry, requiring a defect for its activation – at ~1340 cm^{-1}.[50] Interestingly, a small increase in the intensity ratio of the D and G bands (I_D:I_G) in the CeO_2@GNF nanocomposites relative to GNF was observed, indicating a change in the structural ordering in the graphitic sidewalls of GNF, consistent with the shortening/opening and thermal treatments employed during the preparation of the nanoreactors.[48] In addition, a very weak band at ~450 cm^{-1} is observed in some of the Raman spectra of CeO_2@GNF, consistent with the vibration of the Ce-O bond,[50] confirming the formation of CeO_2. It is important to note that the observed low intensity of CeO_2 vibrations is expected given the large number of graphitic layers comprising the GNF sidewalls that shield the confined CeO_2 nanoparticles, indicating that most of the ceria nanoparticles are encapsulated inside GNF.

Like the Raman spectra, PXRD patterns of CeO_2@GNF (**Figure 2c**) show strong evidence for the presence of GNF in the composite. The diffraction peaks of GNF at 2θ = 26.0, 42.4, 44.6, 54.4 and 77.4° correspond to the (002), (100), (101), (104) and (110) planes of the graphitic lattice,[51] and remain unchanged in CeO_2@GNF. In CeO_2@GNF-1, no significant new peaks corresponding to CeO_2 are observed, which can be attributed to a low amount or very small size of CeO_2 nanoparticles. However, for CeO_2@GNF-3, which contains the highest amount of ceria, the PXRD pattern contains four new peaks at 2θ = 28.3, 32.8, 47.3 and 56.3° corresponding to the (111), (200), (220) and (311) crystal planes of CeO_2 (JCPDS card no. 43-1002), which are less prominent, but still measurable, in CeO_2@GNF-2. The PXRD patterns confirm the crystalline nature of CeO_2, exhibiting a face centred cubic fluorite crystal lattice.[29] For CeO_2@GNF-3, the crystallite size of the CeO_2 can be estimated from the full width half maximum (FWHM) of the (111) peak at 2θ = 28.3° using the Scherrer equation[52] as ~9 nm. Therefore, the fact that CeO_2 peaks are more prominent in CeO_2@GNF-3 is related to the highest content of ceria and thus the increase in the size of CeO_2 nanoparticles, consistent with previous reports.[53]

Although the TGA, Raman spectroscopy and PXRD results all suggest the formation of a nanocomposite of CeO_2 and GNF, the location of CeO_2, i.e. inside or outside GNF, could only be ascertained from transmission electron microscopy (TEM). Interestingly, TEM imaging reveals CeO_2 nanoparticles are well dispersed inside the GNF in all samples (**Figure 3**). At the lowest amount of cerium precursor (1 mg in CeO_2@GNF-1), effectively all CeO_2 nanoparticles are observed to be embedded inside GNF (**Figure 3a**); however, at higher precursor loadings (3 mg in CeO_2@GNF-3), a noticeable, but still minor, number of nanoparticles were found on the outer surface of GNF (**Figure 3c** and S2a and d, SI). This indicates that the best level of control over the location of nanoparticles is achieved with the smallest amount of the precursor complex.

Consistent with previous studies, CeO_2 nanoparticles are found to be preferentially adsorbed at the internal step-edges of GNF (Figures 1, S2b and c, SI). Furthermore, mean diameters of ceria nanoparticles of 4.6±0.2, 6.2±0.6 and 8.5±0.3 nm were determined by TEM for CeO_2@GNF-1, -2 and -3, respectively (insets in **Figures 3a-c**), the latter of which matching well with the size estimated from PXRD, clearly showing the positive correlation between nanoparticle size and precursor concentration.[54] High resolution TEM images (**Figure 3e**) of CeO_2 nanoparticles show clear atomic fringes with interplanar *d*-spacings of 0.32 nm corresponding to the (111) planes of ceria, and EDX spectroscopy analysis identifies Ce and O in the correct stoichiometry for CeO_2@GNF (**Figure 3d**). However, more detailed analysis by XPS (**Figure 2d**) indicates the existence of an oxygen-depleted surface containing both Ce^{4+} (78.8 at%) and Ce^{3+} (21.2 at%) based on deconvolution of the Ce 3d signal (Figure S3 and Tables S1-2, SI).[55,56] The presence of Ce^{3+} is significant for our reaction, as Ce^{3+} is known to be key for initiation of radical-mediated organic transformations.

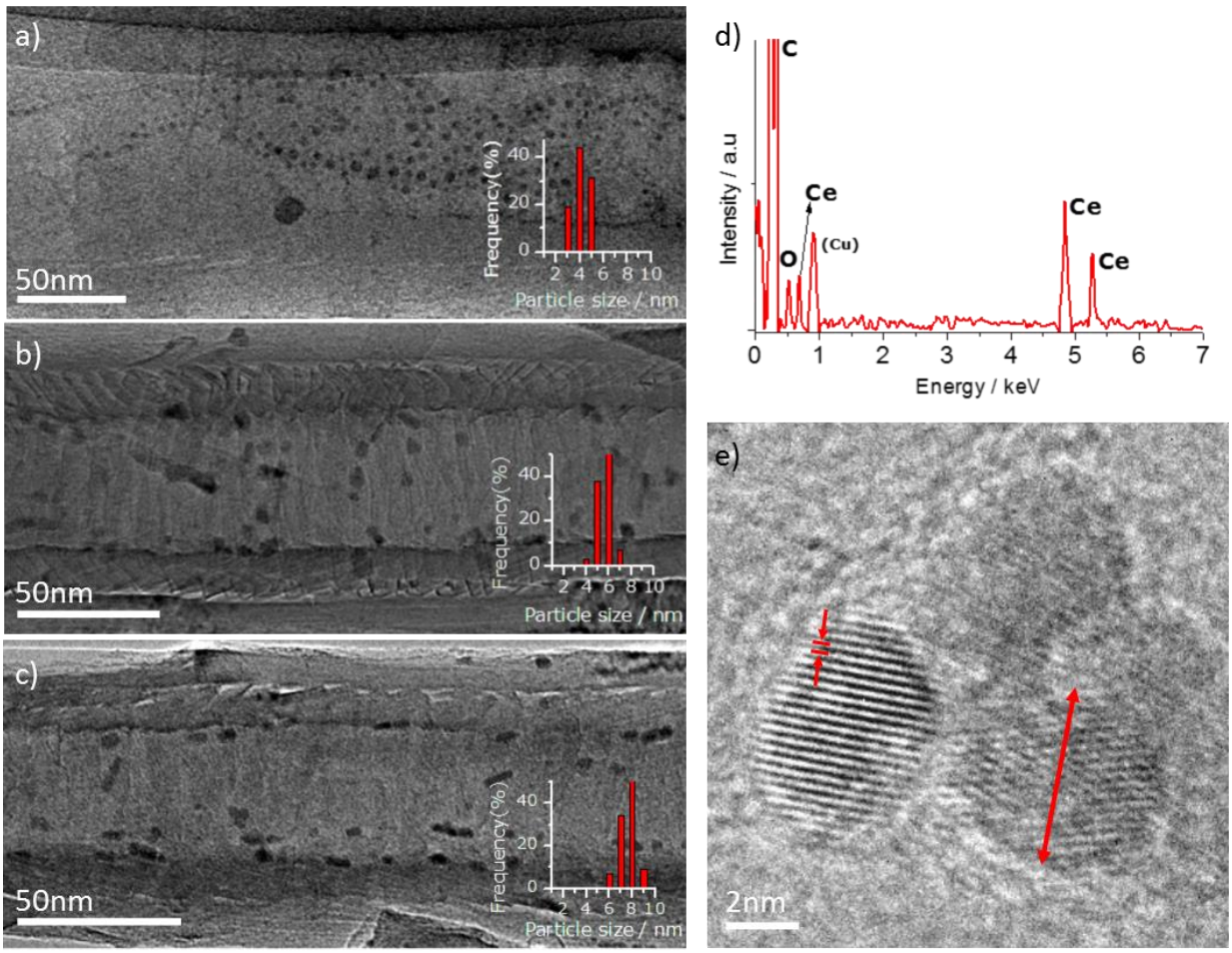

Figure 3. HRTEM analysis of CeO_2 nanoparticles encapsulated inside GNF (CeO_2@GNF). HRTEM images of CeO_2@GNF-1, -2 and -3 (a-c) and corresponding size distribution histograms of CeO_2 nanoparticles (inset). The EDX spectrum of CeO_2@GNF-3 (d) confirms the elemental composition and stoichiometry of Ce and O in CeO_2 (Ce:O is 0.5:1.0). HRTEM images of the CeO_2 nanoparticles encapsulated inside GNF (nanoparticle diameter indicated by the double-headed red arrow) showing *d*-spacing of 0.32 nm (e).

CeO_2@GNF in the oxidation of cyclohexene

The CeO_2@GNF composites were tested as initiators in the oxidation of cyclohexene by *tert*-butylhydroperoxide. This specific reaction was chosen as it is known to proceed through two different routes, either *via* allylic or olefinic oxidation, leading to the formation of five main

products[57-60], with the ratio of these products influenced by the conditions of the reaction, including the oxidant, temperature, time, pressure and solvent.[61,62] Under our experimental conditions of 80 ºC for 9 hours in acetonitrile, the control reaction (entry 1, **Table 1**) gave 18% conversion for cyclohexene with the formation of products *via* both allylic (2-cyclohexenylhydroperoxide (**1**)) and olefinic (cyclohexaneepoxide (**4**)) oxidation pathways in a 50:50 ratio of (**1**):(**4**) indicating low selectivity of this reaction. In the presence of empty GNF (entry 3, **Table 1**), the conversion increased to 45% with the formation of only allylic oxidation products (**1**), (**2**) and (**3**). The observed higher conversion is consistent with the known effect of decomposition of peroxy compounds, here TBHP, in the presence of graphitic carbon surfaces generating reactive oxygen species, i.e. hydroxyl radicals.[63,64] The key effect of the presence of ceria in CeO_2@GNF, as compared to empty GNF, is a significant increase of conversion (up to 94%) with 2-cyclohexenone (**2**) and 2-cyclohexenyl hydroperoxide (**1**) as major products observed for CeO_2@GNF-2 (entry 5, **Table 1** and **Figure 4a**). Comparison of the CeO_2@GNF nanoreactors with different loadings of ceria (CeO_2@GNF-X where X=1,2,3) did not reveal significant differences in terms of cyclohexene conversion (Figure S5 and Table S3, SI). Interestingly, we noted a clear dependence on the specific distribution of products as a function of reaction time using CeO_2@GNF-2 (**Figure 4c**). At 7 hours, the yield of (**1**) is maximal at 89% selectivity (entry 4, **Table 1**), at a high conversion of 88%. As the reaction proceeds, (**1**) is consumed to produce both (**2**) and (**3**), with a conversion of 100% and moderate selectivity of 56% for (**2**) observed at 24 hours (entry 6, **Table 1**). This indicates that the preferred product ((**1**) or (**2**)) can in principle be obtained in high yield and moderate-to-good selectivity simply by stopping the reaction at a user-specified time point.

Table 1. The effects of CeO_2 loading, particle size, reaction time and location in GNF and on graphite and activated carbon on the conversion of cyclohexene and distribution of the afforded products: 2-cyclohexenyl hydroperoxide (**1**), 2-cyclohexenone (**2**), 2-cyclohexenol (**3**), cyclohexane epoxide (**4**) and 1,2-cyclohexanediol (**5**).

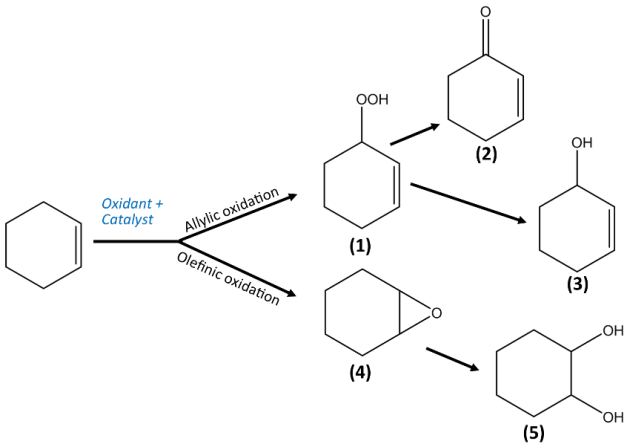

Entry	Species [a]	CeO_2 loading / % [b]	Particle size nm [c]	Reaction time /h	Conversion / % [d]	Selectivity / % (1):(2):(3):(4):(5) [d]
1	None	-	-	9	18	50:0:0:50:0
2 [e]				9	0	0:0:0:0:0
3	GNF	-	-	9	44	60:22:18:0:0
4	CeO_2@GNF-2	5.9	6.2±0.6	7	88	89:11:0:0:0
5				9	94	66:34:0:0:0
6				24	100	28:56:16:0:0
7	CeO_2@graphite	3.7	6.7±1.8	9	30	93:7:0:0:0
8	CeO_2@AC	4.8	4.5±0.8	9	41	84:12:4:0:0

[a] Reaction conditions: cyclohexene (2.9 mmol), TBHP oxidant (5.8 mmol), 1,4-dichlorobenzene internal standard (1.44 mmol), acetonitrile (2.5 mL), 80 °C. [b] Determined by TGA. [c] Determined by TEM. [d] Determined by ^{1}H NMR spectroscopy. [e] Under anaerobic conditions.

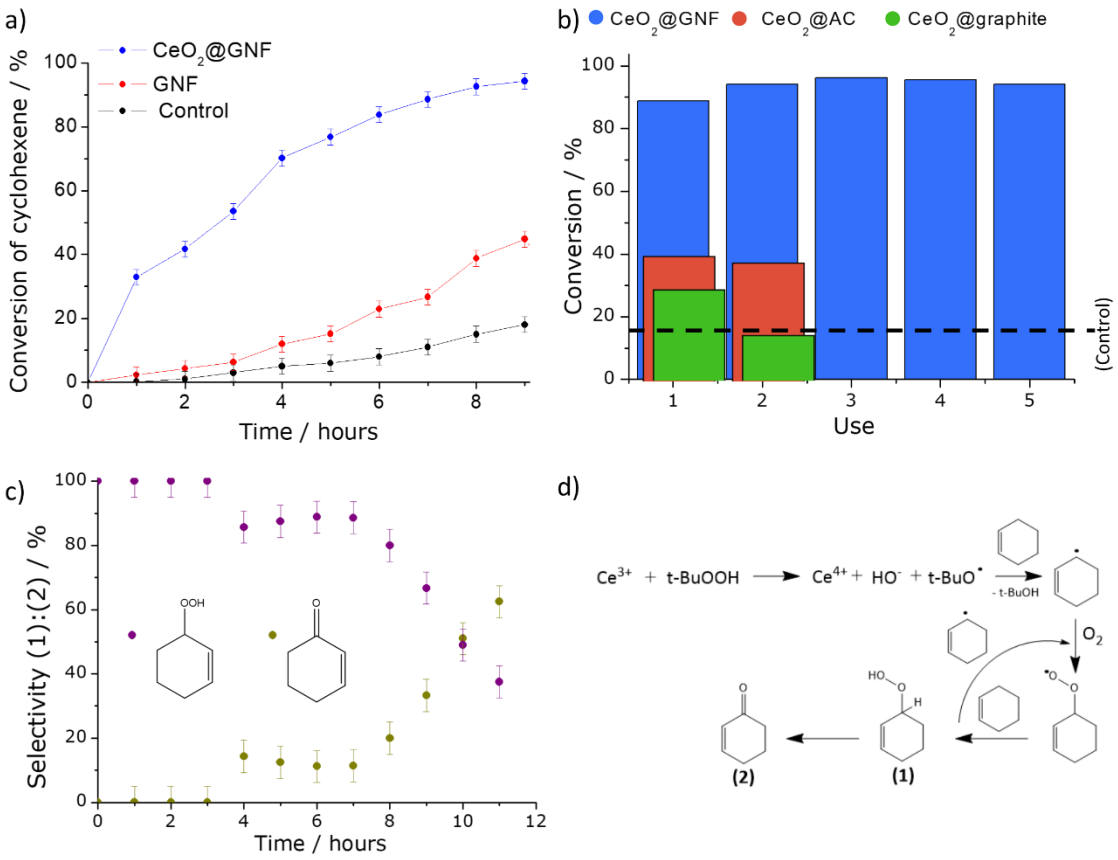

Figure 4. The conversion of cyclohexene obtained using CeO_2@GNF (here CeO_2@GNF-2) relative to control experiments as a function of time (a) and repeat use (b). The dotted horizontal line in (b) represents the conversion obtained in control experiments as reference. The change in selectivity for the products 2-cyclohexenyl hydroperoxide (**1**) and 2-cyclohexenone (**2**) with time (c), demonstrating the user-specificity of product selection using CeO_2@GNF. A proposed pathway for the oxidation of cyclohexene by ceria in CeO_2@GNF; Ce^{3+} reacting with the peroxide reagent triggers a flux of radicals initiating a cycle of reactions with O_2 biradical leading to compound (**1**) which subsequently transforms to (**2**) (d).

It is important to note that the lack of products from the olefinic oxidation pathway differs significantly from previous reports on the oxidation of cyclohexene with TBHP using CeO_2 nanoparticles, where a mixture of (**2**), (**3**) and (**4**) were identified as major products (Table S4, SI).[65] In addition, Voort *et al.*[66] reported the formation of both (**4**) and (**1**) as products of cyclohexene oxidation by TBHP, suggesting the reaction proceeds through both allylic and olefinic

oxidation pathways. Moreover, it should be highlighted that our nanoreactors CeO_2@GNF have very small ceria loadings (0.13 mol%) (Table S4, SI) compared to previous reports (by more than two orders of magnitudes in some instances), with up to 95 wt% of CeO_2 in CeO_2/VO_2 – more a stoichiometric reactant than a catalyst – required to bring about effective oxidation.[65]

In order to study the stability, and thus recyclability, of CeO_2@GNF, we have evaluated the cyclohexene conversion using CeO_2@GNF over five uses. After each use, the catalyst was filtered and washed repeatedly with methanol and kept overnight at 65^{o}C in air. The conversion of cyclohexene was found to subtly increase from the first to the third use, with a very small decrease observed thereafter (**Figure 4b**). The increase in conversion after the first use can be attributed to the cleaning of the nanoparticle surface under the reaction conditions.[67] TGA profiles of fresh and recycled CeO_2@GNF (Figure S4, SI) shows no significant loss of CeO_2 content even after five uses, indicating good stability of CeO_2@GNF to leaching.

The enhanced cyclohexene conversion observed with CeO_2@GNF, and its associated stability towards repeat use, can be attributed to the effects of spatial confinement of CeO_2 inside GNF. This has been shown to lead to: (i) well dispersed CeO_2 nanoparticles of very small diameter (3-8 nm), protected at the graphitic step-edges from deactivation mechanisms, yet providing a large surface area for the adsorption of reactant molecules; (ii) increased local concentration of reactants inside nanoreactors promoting the effective interaction between reactant molecules and CeO_2, thus improving conversion and (iii) easy diffusion of reactant and product molecules to and from the nanoreactor, while maintaining strong local interactions with the CeO_2 nanoparticles at the GNF step-edges. These effects are consistent with the spatial confinement observed for other nanoparticles inside carbon nanoreactors, including GNF, that often result in highly selective organic transformations use-to-use.[25,26]

The importance of confinement

To validate the importance of step-edges and nanoscale confinement inside GNF on the functional properties of ceria, CeO_2 nanoparticles were separately deposited onto activated carbon (AC) and graphite flakes (Figure S6, SI). AC and graphite both provide anchoring sites for nanoparticles, akin to GNF, but no spatial restrictions as inside the GNF cavity. TEM analysis (Figure S6c-g, SI) indicates that ceria nanoparticles on AC and graphite are uniformly distributed on both carbons and are qualitatively similar in size to those observed in CeO_2@GNF. A preference for cubic morphology was noted for CeO_2 on graphite. Interestingly, TGA (Figure S6a,b) shows clear differences in the combustion temperature of the carbon supports after deposition of ceria: a significant reduction (by more than 200 ºC) was observed for AC; only a minimal difference was recorded using graphite. This suggests a higher intimacy of contact between CeO_2 and AC, like that observed using GNF, relative to graphite where contact is poorer. However, ^{1}H NMR spectroscopy analysis indicates lower conversion in the oxidation of cyclohexene using both CeO_2@AC and CeO_2@graphite relative to CeO_2@GNF (entries 7, 8 and 5, respectively, **Table 1**). Moreover, whilst cyclohexene conversion is largely retained after the first use of CeO_2@AC, this drops significantly when using CeO_2@graphite (**Figure 3b**) indicating low stability, and thus recyclability, of ceria on this carbon support. Thus, whilst we cannot rule out additional factors that may contribute to the observed reactivity and stability of CeO_2@GNF, these observations suggest the importance of nanoscale confinement inside GNF nanoreactors, providing a new way to enhance cyclohexene conversion, use-to-use, whilst simultaneously improving the selectivity for allylic oxidation at very low loadings.

Mechanistic considerations

Based on our results and previous literature concerning the TBHP-mediated oxidation in the presence of CeO_2 and transition metals[68-70], a plausible mechanism for the oxidation of cyclohexene can be proposed (**Figure 4d**). Since no epoxide is detected during the reaction, the formation of products through the selective oxidation of the allylic carbon centre by free radicals appears the most viable option. Our XPS measurement demonstrated that ~20% of cerium cations in CeO_2@GNF are in oxidation state Ce^{3+}. The redox reaction of Ce^{3+} centres with t-BuOOH yields t-BuO$^{\cdot}$ radicals, similar to the process described for other nanoscale materials.[71-73] The free radical t-BuO$^{\cdot}$ extracts the allylic hydrogen from cyclohexene to form the cyclohexenyl radical, which becomes trapped by atmospheric O_2 to form 2-cyclohexenyl peroxide radical.[74,75] The critical role of atmospheric oxygen was ascertained in control experiments, under anaerobic conditions, where negligible conversion was observed (entry 2, **Table 1**). The 2-cyclohexenyl peroxide radical subsequently abstracts hydrogen from the allylic CH_2 of another molecule of cyclohexene to form 2-cyclohexenyl hydroperoxide (**1**),[76,77] the existence of which is confirmed by ^{1}H NMR spectroscopy. This homolytic abstraction of hydrogen is also energetically favourable: the bond energies of RO-H and the allylic C-H bond are 90 and 85 kcal mol^{-1}, respectively.[78] In effect, ceria nanoparticles act as an initiator of the free-radical allylic oxidation cycle which then continues producing (**1**) which in turn forms (**2**). The low amount of HO$^{\cdot}$ radicals in this process explain the low yield of product (**3**), only observed after extensive heating, which forms without ceria in GNF on shorter timescales.

Analysis of CeO_2@GNF after the reaction offers additional mechanistic insights. XPS shows no significant changes in the ratio between Ce^{4+} (78.1%) and Ce^{3+} (21.9%), but a shift of ca. 1 eV towards higher binding energy in all Ce 3d components. The shift is likely to be associated with the presence of hydroxyl groups on ceria after the reaction (bi-product of peroxide decomposition; Figure 3d), which corroborates with a large increase of the O 1s peak at ca. 532 eV associated to hydroxyl groups (Figure S3d, SI). This suggests that GNF acts as an electron reservoir compensating for the loss of electrons in ceria, as observed previously for other metal compounds inside carbon nanotubes,[79,80] effectively restoring the Ce^{4+}/Ce^{3+} balance.

CONCLUSIONS

A method for the preparation of very small CeO_2 nanoparticles encapsulated inside graphitised carbon nanofibres by gas phase thermal decomposition of cerium complex [$Ce(tmhd)_4$] has been developed. The average size of CeO_2 nanoparticles inside GNF can be tuned from ~4 to 9 nm by adjusting the ratio of the precursor complex to GNF. CeO_2 nanoparticles deposited at the graphitic step-edges of GNF promote cyclohexene oxidation, demonstrating a significantly improved conversion and exclusive selectivity towards allylic oxidation products as compared to previously reported ceria nanomaterials. Analysis of the product distribution with and without CeO_2 in GNF suggests that the allylic pathway of the reaction is dictated by the carbon nanoreactor itself while the presence of cerium oxide enhances the efficiency of the nanoreactor CeO_2@GNF leading to higher conversion, playing the essential role of initiator in the production of cyclohexenyl hydroperoxide. Furthermore, comparison of CeO_2@GNF nanoreactors with different sizes of ceria nanoparticles demonstrated that ~6 nm nanoparticles are most active and deliver the highest yield

of 2-cyclohexenone. Investigations of the oxidation reactions with nanoparticles not confined to nanoscale volumes highlight the ability of the GNF to enhance cyclohexene conversion, whilst simultaneously improving the selectivity for the allylic oxidation at low loadings, and maintaining the balance of oxidation states in ceria by effectively acting as a reservoir of electrons. Importantly, these nanoreactors CeO_2@GNF could also be easily separated from the reaction mixture and reused, largely retaining their performance over at least five uses. This factor makes these nanoreactors a suitable candidate for the sustainable use of lanthanide-based materials in preparative organic synthesis.

ASSOCIATED CONTENT

Supporting Information. This material is available free of charge on the ACS publications website.

AUTHOR INFORMATION

Corresponding Author

*School of Chemistry, University of Nottingham, University Park, Nottingham, NG7 2RD, UK. E-mail: Maxwell.Astle@nottingham.ac.uk; Andrei.Khlobystov@nottingham.ac.uk; Fax: +44 (0) 115 9513563; Tel: +44 (0) 115 9513917

Present Addresses: †Department of Chemistry, Deen Dayal Upadhyaya College, University of Delhi, New Delhi. 1100078, India. Fax: +91-11-25099380, Tel: +91-11-25099381

Author Contributions

The manuscript was written through the contributions of all authors. All authors have given approval to the final version of the manuscript.

Funding Sources

The work was supported by the University of Delhi, India, the Engineering and Physical Research Council (EPSRC) and the Centre for Sustainable Chemistry, University of Nottingham.

Notes

The authors declare no competing financial interest.

ACKNOWLEDGMENT

NA acknowledges the financial support provided by the University of Delhi, India to carry out the work at the University of Nottingham. We also acknowledge the Nanoscale Microscale Research Centre (nmRC) for TEM and Raman analysis. MAA, GAR and ANK acknowledge the Engineering and Physical Research Council (EPSRC) and Advanced Molecular Materials Research Priority Area (University of Nottingham) for funding, and the Centre for Sustainable Chemistry (CSC), University of Nottingham, for access to analytical facilities.

ABBREVIATIONS

GNF, graphitised carbon nanofibre; CNT, carbon nanotubes; $Ce(tmhd)_4$, tetrakis(2,2,6,6-tetramethyl-3,5-heptanedionato) cerium (IV); HRTEM, high resolution transmission electron microscopy; EDX, energy dispersive X-ray spectroscopy; TGA, thermogravimetric analysis;

PXRD, powder x-ray diffraction; XPS, X-ray photoelectron spectroscopy; TBHP, tert-Butyl hydroperoxide.

REFERENCES

(1) Yamamoto, H.; Shibasaki, M.; Yamada, K. I.; Yoshikawa, N. Lewis acids in organic synthesis; Wiley VCH: Weinheim, 2008.

(2) Benelli, C.; Gatteschi, D. Magnetism of Lanthanides in Molecular Materials with Transition-Metal Ions and Organic Radicals. *Chem. Rev.*, **2002**, *102* (6), 2369–2388.

(3) Park, J. Y.; Chang, Y.; Lee, G. H. Multi-Modal Imaging and Cancer Therapy Using Lanthanide Oxide Nanoparticles: Current Status and Perspectives. *Curr. Med. Chem.* **2015**, 22, 569−581.

(4) Aspinall, H. C. Chemistry of the f –Block Elements, Gordon & Breach Sc. Publishers, Canada, 2001.

(5) Phokha, S.; Pinitsoontorn, S., Chirawatkul, P., Poo-arporn, Y.; Maensiri, S. Synthesis, characterization, and magnetic properties of monodisperse CeO_2 nanospheres prepared by PVP-assisted hydrothermal method. *Nanoscale Res. Lett.*, **2012**, *7*, 425, 1-13.

(6) Choudhury, B.; Chetri, P.; Choudhury, A. Oxygen defects and formation of Ce^{3+} affecting the photocatalytic performance of CeO_2 nanoparticles. *RSC Adv.*, **2014**, *4*, 4663-4671.

(7) Chen, G.; Xu, C.; Song, X.; Zhao, W.; Ding, Y.; Sun, S. Interface Reaction Route to Two Different Kinds of CeO_2 Nanotubes. *Inorg. Chem.*, **2008**, *47*, 723–728.

(8) Sun, Z.; Zhang, H., An, G.; Yang, G.; Liu, Z. Supercritical CO_2-facilitating large-scale synthesis of CeO_2 nanowires and their application for solvent-free selective hydrogenation of nitroarenes. *J. Mater. Chem.,* **2010**, *20*, 1947-1952.

(9) Sun, C.; Chen, L.Controllable Synthesis of Shuttle-Shaped Ceria and Its Catalytic Properties for CO Oxidation. *Eur. J. Inorg. Chem.*, **2009**, *26*, 3883−3887.

(10) Trovarelli, A. Ceria and Related Materials (Ed.: A. Trovarelli), Imperial College Press, London, 2002.

(11) Imagawa, H.; Suda, A.; Yamamura, K; Sun, S. Monodisperse CeO_2 Nanoparticles and Their Oxygen Storage and Release Properties. *J. Phys. Chem. C*, **2011**, *115* (5), 1740–1745.

(12) Tamura, M.; Tomishige, K. Redox Properties of CeO_2 at Low Temperature: The Direct Synthesis of Imines from Alcohol and Amine. *Angew. Chem. Int. Ed.*, **2015**, *54*, 864-867.

(13) Guzman, J.; Carrettin, S.; Fierro-Gonzalez, J. C.; Hao, Y. L.; Gates, B. C.; Corma, A. CO Oxidation Catalyzed by Supported Gold: Cooperation between Gold and Nanocrystalline Rare-Earth Supports Forms Reactive Surface Superoxide and Peroxide Species. *Angew. Chem. Int. Ed.*, **2005**, *44*, 4778-4781.

(14) Yang, X.; Kattel, S.; Senanayake, S. D.; Boscoboinik, J. A.; Nie, X.; Graciani, J.; Rodriguez,´ J.A.; Liu, P.; Stacchiola, D. J.; Chen, J. G. Low Pressure CO_2 Hydrogenation to Methanol over Gold Nanoparticles Activated on a CeO_x/TiO_2 Interface. *J. Am. Chem. Soc.*, **2015**, *137*, 10104−10107.

(15) Macedo, A. G.; Fernandes, S. E. M.; Valente, A. A.; Ferreira, R. A. S.; Carlos, L. D.; Rocha, J. Catalytic performance of ceria nanorods in liquid-phase oxidations of hydrocarbons with tert-butyl hydroperoxide. *Molecules*, **2010**, *15*, 747-765.

(16) Imanaka. N.; Masui, T.; Jyoko, K. Selective liquid phase oxidation of cyclohexane over Pt/CeO_2-ZrO_2-SnO_2/SiO_2 catalysts with molecular oxygen. *J. Adv. Ceram,* **2015**, *4*, 111–117.

(17) Pirmohamed, T.; Dowding, J. M.; Singh, S.; Wasserman, B.; Heckert, E.; Karakoti, A. S.; King, J. E. S.; Seal, S.; Self, W. T. Nanoceria exhibit redox state-dependent catalase mimetic activity. *Chem. Commun.* **2010**, *46*, 2736–2738.

(18) Xu, C.; Qu, X. Cerium oxide nanoparticle: a remarkably versatile rare earth nanomaterial for biological applications. *NPG Asia Mater*, **2014**, *6*, 90.

(19) Kim, C. R.; Uemura, T.; Kitagawa, S. Fabrication of Ceria Nanoparticles Incorporated in Porous Coordination Polymer. *Chem. Lett.*, **2014**, *43*, 1749–1751.

(20) Zhao, X.; Li, H.; Zhang, J.; Shi, L.; Zhang, D. Design and synthesis of NiCe@ m-SiO2 yolk-shell framework catalysts with improved coke-and sintering-resistance in dry reforming of methane. *Int. J. Hydrogen Energy,* **2016**, *41*, 2447-2456.

(21) Khlobystov, A. N. Carbon Nanotubes: From Nano Test Tube to Nano-Reactor. *ACS Nano*, **2012**, *5*, 9306-9312.

(22) Pan, X.; Bao, X. The effects of confinement inside carbon nanotubes on catalysis. *Acc. Chem. Res.,***2011**, *44*, 553–562.

(23) Torre, A. L.; Gimenez-Lopez, M. d.C.; Fay, M. W.; Rance, G. A.; Solomonsz, W. A.; Chamberlain, T. W.; Brown, P.D.; Khlobystov, A. N. Assembly, Growth, and Catalytic Activity of Gold Nanoparticles in Hollow Carbon Nanofibers. *ACS Nano*, **2012**, *6* (3), 2000–2007.

(24) Solomonsz,W. A.; Rance, G. A.; Suyetin, M.; Torre, A. L.; Bichoutskaia, E.; Khlobystov, A. N. Controlling the Regioselectivity of the Hydrosilylation Reaction in Carbon Nanoreactors. *Chem. Eur. J.*, **2012**, *18*, 13180-13187.

(25) Wang, J; Lu, S.M; Li, J; Li, C. A remarkable difference in CO_2 hydrogenation to methanol on Pd nanoparticles supported inside and outside of carbon nanotubes. *Chem. Commun.* **2015**, *51*, 17615-17618.

(26) Zhang, X; Guo; Y.C; Zhang, Z.C; Gao, J.S; Xu C.M. High performance of carbon nanotubes confining gold nanoparticles for selective hydrogenation of 1,3-butadiene and cinnamaldehyde. *J. Catal,* **2012**, *292*, 213–226.

(27) Chen, X.; Gao, S.; Wang, H.; Liu, Y.; Wu, Z. Selective catalytic reduction of NO over carbon nanotubes supported CeO_2. *Catal. Commun*, **2011**, *14*, 1–5.

(28) Zhang, D.; Zhang, L.; Shi, L.; Fang, C.; Li, H.; Gao, R; Huang, L.; Zhang, J. In situ supported MnO_x–CeO_x on carbon nanotubes for the low-temperature selective catalytic reduction of NO with NH_3. *Nanoscale*, **2013**, *5*, 1127.

(29) Qiu, J.D.; Cui, S. G.; Liang, R. P. Hydrogen peroxide biosensor based on the direct electrochemistry of myoglobin immobilized on ceria nanoparticles coated with multiwalled carbon nanotubes by a hydrothermal synthetic method. *Microchim Acta*, **2010**, *171*, 333–339.

(30) Li, Y.; Liu, X. R.; Ning, X. H.; Huag, C. C.; Zheng, J. B.; Zhang, J. C. An ionic liquid supported CeO_2 nanoparticles–carbon nanotubes composite-enhanced electrochemical DNA-based sensor for the detection of Pb^{2+}. *J. Pharm. Anal*, **2011**, *1*, 258–263.

(31) Selvan,V. A. M.; Anand, R.B.; Udayakumar, M. Effect of Cerium Oxide Nanoparticles and Carbon Nanotubes as fuel-borne additives in Diesterol blends on the performance, combustion and emission characteristics of a variable compression ratio engine. *Fuel*, **2014**, *130*, 160–167.

(32) Raoa, R.; Zhang, Q., Liu, H.; Yang, H.; Ling, Q.; Yang, M.; Zhang, A.; Chen, W. Enhanced catalytic performance of CeO_2 confined inside carbon nanotubes for dehydrogenation of ethylbenzene in the presence of CO_2. *J. Mol. Catal. A: Chemical* **2012**, *363–364*, 283–290.

(33) Astle, M. A.; Rance, G. A.; Loughlin, H.; Peters, T. D.; Khlobystov, A. N., Molybdenum Dioxide in Carbon Nanoreactors as a Catalytic Nanosponge for the Efficient Desulfurization of Liquid Fuels. *Adv. Funct. Mater.* **2019**, 29, 1808092.

(34) Solomonsz, W. A.; Rance, G. A.; Khlobystov, A. N. Evaluating the Effects of Carbon Nanoreactor Diameter and Internal Structure on the Pathways of the Catalytic Hydrosilylation Reaction. *Small,* **2014**, *10*, 1866–1872.

(35) Gimenez-Lopez, M. d. C.; Kurtoglu, A.; Walsh, D. A.; Khlobystov, A. N. Extremely Stable Platinum-Amorphous Carbon Electrocatalyst within Hollow Graphitized Carbon Nanofibers for the Oxygen Reduction Reaction. *Adv. Mater.* **2016**, *28*, 9103-9108.

(36) Astle, M. A.; Rance. G. A.; Fay, M. W.; Notman, S.; Sambrook, M. R.; Khlobystov, A. N. Synthesis of hydroxylated group IV metal oxides inside hollow graphitised carbon nanofibers:

nanosponges and nanoreactors for enhanced decontamination of organophosphates. *J. Mater. Chem. A*, **2018**, *6*, 20444-20453.

(37) Castillejos, E.; Debouttiere, P. J.; Roiban, L.; Solhy, A.; Martinez, V.; Kihn, Y.; Ersen, O.; Philippot, K.; Chaudret, B.; Serp, P., An Efficient Strategy to Drive Nanoparticles into Carbon Nanotubes and the Remarkable Effect of Confinement on Their Catalytic Performance. *Angew. Chem.-Int. Edit.* **2009**, *48 (14)*, 2529-2533.

(38) La Torre, A.; Gimenez-Lopez, M. D.; Fay, M. W.; Rance, G. A.; Solomonsz, W. A.; Chamberlain, T. W.; Brown, P. D.; Khlobystov, A. N., Assembly, Growth, and Catalytic Activity of Gold Nanoparticles in Hollow Carbon Nanofibers. *ACS nano,* **2012**, *6 (3)*, 2000-2007.

(39) Castillejos, E.; Jahjah, M.; Favier, I.; Orejon, A.; Pradel, C.; Teuma, E.; Masdeu-Bulto, A. M.; Serp, P.; Gomez, M., Synthesis of Platinum-Ruthenium Nanoparticles under Supercritical CO2 and their Confinement in Carbon Nanotubes: Hydrogenation Applications. *ChemCatChem* **2012**, *4 (1)*, 118-122.

(40) Tessonnier, J. P.; Pesant, L.; Ehret, G.; Ledoux, M. J.; Pham-Huu, C., Pd nanoparticles introduced inside multi-walled carbon nanotubes for selective hydrogenation of cinnamaldehyde into hydrocinnamaldehyde. *Appl. Catal., A*, **2005**, *288 (1-2)*, 203-210.

(41) Zhang, J.; Muller, J. O.; Zheng, W. Q.; Wang, D.; Su, D. S.; Schlogl, R., Individual Fe-Co alloy nanoparticles on carbon nanotubes: Structural and catalytic properties. *Nano Lett*. **2008**, *8 (9)*, 2738-2743.

(42) Li, X. J.; Zhang, L. P.; Tan, R. P.; Fazzini, P. F.; Hungria, T.; Durand, J.; Lachaize, S.; Sun, W. H.; Respaud, M.; Soulantica, K.; Serp, P., Isoprene Polymerization on Iron Nanoparticles Confined in Carbon Nanotubes. *Chem.: Eur. J.* **2015**, *21 (48)*, 17437-17444.

(43) Rance, G. A.; Solomonsz, W. A.; Khlobystov, A. N., Click chemistry in carbon nanoreactors. *Chem. Commun.* **2013**, *49 (11)*, 1067-1069.

(44) Lebedeva, M. A.; Chamberlain, T. W.; Schroder, M.; Khlobystov, A. N., New Pathway for Heterogenization of Molecular Catalysts by Non-covalent Interactions with Carbon Nanoreactors. *Chem. Mater.* **2014**, *26 (22)*, 6461-6466.

(45) Lebedeva, M. A.; Chamberlain, T. W.; Thomas, A.; Thomas, B. E.; Stoppiello, C. T.; Volkova, E.; Suyetin, M.; Khlobystov, A. N., Chemical reactions at the graphitic step-edge: changes in product distribution of catalytic reactions as a tool to explore the environment within carbon nanoreactors. *Nanoscale*, **2016**, *8 (22)*, 11727-11737.

(46) Aygun, M.; Chamberlain, T. W.; Gimenez-Lopez, M. D.; Khlobystov, A. N., Magnetically Recyclable Catalytic Carbon Nanoreactors. *Adv. Funct. Mater.* **2018**, *28 (34)*, 15.

(47) Cornelio, B.; Saunders, A. R.; Solomonsz, W. A.; Laronze-Cochard, M.; Fontana, A.; Sapi, J.; Khlobystov, A. N.; Rance, G. A., Palladium nanoparticles in catalytic carbon nanoreactors: the effect of confinement on Suzuki-Miyaura reactions. *J. Mater. Chem.* **2015**, *3 (7)*, 3918-3927.

(48) Chamberlain, T. W.; Zoberbier, T.; Biskupek, J.; Botos, A.; Kaiser, U.; Khlobystov, A. N. Formation of uncapped nanometre-sized metal particles by decomposition of metal carbonyls in carbon nanotubes. *Chem. Sci.*, **2012**, *3*, 1919-1924.

(49) Beltram, A.; Melchionna, M.; Montini, T.; Nasi, L.; Gorte, R.J.; Prato, M.; Fornasiero, P. Improved activity and stability of Pd@CeO_2 core–shell catalysts hybridized with multi-walled carbon nanotubes in thewater gas shift reaction. *Catal. Today*, **2015**, *253*, 142–148.

(50) Cargnello, M.; Grzelczak, M.; Gonzalez, B. R.; Syrgiannis, Z.; Bakhmutsky, K.; Parola, V. L.; Liz-Marzan, L. M.; Gorte, R. J.; Prato, M.; Fornasiero, P. Multiwalled Carbon Nanotubes Drive the Activity of Metal@oxide Core–Shell Catalysts in Modular Nanocomposites. *J. Am. Chem. Soc.*, **2012**, *134*, 11760−11766.

(51) Zhou, O.; Fleming, R.M.; Murphy, D.W.; Chen, C.H.; Haddon, R.C.; Ramirez, A.P.; Glarum, S.H. Defects in carbon nanostructures. *Science*, **1994**, *263*, 1744–1747.

(52) Cullity, B. D.; Stock, S. R. *Elements of X-ray Diffraction* (Prentice Hall, Upper Saddle River, NJ, 2001) 3rd ed.

(53) Azadi, P.; Farnood, R.; Meier, E. Preparation of Multiwalled Carbon Nanotube-Supported Nickel Catalysts Using Incipient Wetness Method. *J. Phys. Chem. A,* **2010**, *114,* 3962–3968.

(54) Vega-Chacón , J.; Picasso; G.; Avilés-Félix, L.; Jafelicci Jr, M. Influence of synthesis experimental parameters on the formation of magnetite nanoparticles prepared by polyol method, *Adv. Nat. Sci.: Nanosci. Nanotechnol*, **2016**, *7*, 015014 (1-7).

(55) Wang, N.; Qian, W.; Chu, W.; Wei, F. Crystal-plane effect of nanoscale CeO2 on the catalytic performance of Ni/CeO2 catalysts for methane dry reforming. *Cat. Sci. Technol.*, **2016**, *6*, 3594-3605.

(56) Rajendran, S.; Khan, M.M.; Gracia, F.; Qin, J.; Gupta, V.K.; Arumainathan, S. Ce^{3+}-ion-induced visible-light photocatalytic degradation and electrochemical activity of ZnO/CeO_2 nanocomposite. *Sci Rep.*. **2016,** *6*, 31641.

(57) Ameur, N.; Bedrane, S.; Bachir, R.; Brham, A. C. Influence of nanoparticles oxidation state in gold based catalysts on the product selectivity in liquid phase oxidation of cyclohexene. *J. Mol. Catal. A: Chemical*, **2013**, *374–375*,1– 6.

(58) Cao, Y.; Yu, H.; Peng, F.; Wang, H. Selective Allylic Oxidation of Cyclohexene Catalyzed by Nitrogen-Doped Carbon Nanotubes. *ACS Catal.*, **2014**, *4*, 1617−1625.

(59) McAteer, B.; Beattie, N.; Richens, D. T. Catalytic oxidation of cyclohexene by aqueous iron(III)/H_2O_2 in mildly acidic solution: Epoxidation versus allylic oxidation. *Inorg. Chem. Commun*, **2013**, *35*, 284–289.

(60) Zhang, R.; Tang, R. Expanded graphite supported copper catalyst for effective oxidation of cyclohexene with molecular oxygen under mild conditions.*J Mater Sci.*, **2016**, *51*, 5802–5810.

(61) Ganji, S.; Bukya, P.; Vakati, V.; Rao, K. S. R.; Burri, D, R. Highly efficient and expeditious PdO/SBA-15catalysts for allylic oxidation of cyclohexene to cyclohexenone. *Catal. Sci. Technol.,* **2013**, *3*, 409-414.

(62) Weiner, H.; Trovarelli, A.; Finke, R. G. Expanded product, plus kinetic and mechanistic, studies of polyoxoanion-based cyclohexene oxidation catalysis: the detection of ∼70 products at higher conversion leading to a simple, product-based test for the presence of olefin autoxidation. *J. Mol. Catal. A: Chemical*, **2003**, *191*, 217–252.

(63) Song, S.; Yang, H.; Rao, R.; Liu, H.; Zhang, A. Defects of multi-walled carbon nanotubes as active sites for benzene hydroxylation to phenol in the presence of H_2O_2. *Catal. Commun.*, **2010**, *11*, 783–787.

(64) Cao, Y.; Luo, X.; Yu, H.; Peng, F.; Wang, H.; Ning, G. sp2- and sp3-hybridized carbon materials as catalysts for aerobic oxidation of cyclohexane. *Catal. Sci. Technol.* **2013**, *3*, 2654−2660.

(65) Korso, S. E.; Bedrane, S.; Braham, A. C.; Bachir, R. The effect of redox properties of ceria-supported vanadium oxides in liquid phase cyclohexene oxidation. *RSC Adv.* **2015**, *5*, 63382–63392.

(66) Leus, K.; Muylaert, I.; Vandichel, M.; Marin, G. B.; Waroquier, M.; Speybroeck , V. V.; Voort, P. V. D.The remarkable catalytic activity of the saturated metal-organic framework V-MIL-47 in the cyclohexene oxidation. *Chem. Commun.*, **2010**, *46*, 5085–5087.

(67) Rui, Z.; Wu, S.; Ji, H.; Liu, Z. Reactivation and Reuse of Platinum-Based Spent Catalysts for Combustion of Exhaust Organic Gases, *Chem. Eng. Technol.* **2015**, *38*, 409-415.

(68) Pathan, S.; Patel, A. Keggin type transition metal substituted phosphomolybdates: heterogeneous catalysts for selective aerobic oxidation of alcohols and alkenes under solvent free condition. *Catal. Sci. Technol.*, **2014**, *4*, 648-656.

(69) García-Cabeza, A.L.; Marín-Barrios, R.; Moreno-Dorado, F.J.; Ortega, M.J.; Massanet, G.M.; Guerra, F.M. Allylic Oxidation of Alkenes Catalyzed by a Copper−Aluminum Mixed Oxide. *Org. Lett.*, **2014**, *16*, 1598−1601.

(70) Yu, P.; Zhou, Y.; Yang, Y.; Tang, R. Two catalytic systems of L-proline/Cu(II) catalyzed allylic oxidation of olefins with tert-butyl hydroperoxide. *RSC Adv.*, **2016**, *6*, 65403-65411.

(71) Hiatt, R.; Mill, T.; Mayo, F. R. Homolytic decompositions of hydroperoxides. I. Summary and implications for autoxidation. *J. Org. Chem.*, **1968**, *33*, 1416-1420.

(72) Cancino, P.; García, V. P.; Aguirre, P.; Spodine, E. A reusable CuII based metal–organic framework as a catalyst for the oxidation of olefins. *Catal. Sci. Technol.*, **2014**, *4*, 2599–2607.

(73) Cabeza, A. L. G.; Barrios, R. M.; Dorado, F. J. M.; Ortega, M. J.; Massanet, G. M.; Guerra, F. M. Allylic Oxidation of Alkenes Catalyzed by a Copper–Aluminum Mixed Oxide. *Org. Lett.* **2014**, *16*, 1598−1601.

(74) Chen, Z.; Luck, R. L. Oxidation of olefins using atmospheric oxygen atoms initiated by *tert*-butylhydroperoxide or hydrogen peroxide with silver nanoparticles deposited on MCM-41 as catalysts. *Green Chem.*, **2016**, *18*, 3354–3359.

(75) Zarghani, M.; Akhlaghinia, B. Fe_3O_4 magnetic nanoparticles (MNPs) as an efficient catalyst for selective oxidation of benzylic and allylic C–H bonds to carbonyl compounds with *tert*-butyl hydroperoxide. *RSC Adv.*, **2016**, *6*, 38592–38601.

(76) Bai, L.; Yao, L.; Yang Y.; Lee, J. M. Microspheres with Au@SiO_2 core and mesoporous aluminosilica shell as superior heterogeneous catalysts for the aerobic epoxidation of *cis*-cyclooctene. *Chem. Commun.,* **2015**, *51*, 4259–4262.

(77) Bawaked, S.; Dummer, N. F.; Bethell, D.; Knight, D. W.; Hutchings, G. J. Solvent-free selective epoxidation of cyclooctene using supported gold catalysts: an investigation of catalyst re-use. *Green Chem.*, **2011**, *13*, 127–134.

(78) Vincent, J.M.; Rabion, A. ; Yachandra V. K.; Fish, R. H. Fluorous Biphasic Catalysis: Complexation of 1,4,7-[$C_8F_{17}(CH_2)_3]_3$-1,4,7-Triazacyclononane with [$M(C_8F_{17}(CH_2)_2CO_2)_2$] (M = Mn, Co) To Provide Perfluoroheptane-Soluble Catalysts for Alkane and Alkene Functionalization in the Presence of *t*-BuOOH and O_2. *Angew. Chem. Int. Ed.*, **1997**, *36*, 2346-2349.

(79) Botos, A.; Biskupek, J.; Chamberlain, T. W.; Rance, G. A.; Stoppiello, C. T.; Sloan, J.; Liu, Z.; Suenaga, K.; Kaiser, U.; Khlobystov, A. N., Carbon Nanotubes as Electrically Active Nanoreactors for Multi-Step Inorganic Synthesis: Sequential Transformations of Molecules to Nanoclusters and Nanoclusters to Nanoribbons. *J. Am. Chem. Soc.* **2016,** *138* (26), 8175-8183.

(80) Jordan, J. W.; Lowe, G. A.; McSweeney, R. L.; Stoppiello, C. T.; Lodge, R. W.; Skowron, S. T.; Biskupek, J.; Rance, G. A.; Kaiser, U.; Walsh, D. A.; Newton, G. N.; Khlobystov, A. N., Host-Guest Hybrid Redox Materials Self-Assembled from Polyoxometalates and Single-Walled Carbon Nanotubes. Adv. Mater. 2019, 31 (41), 5.

TOC Graphic